ACS APPLIED MATERIALS & INTERFACES

Research Article

www.acsami.org

Preferred Molecular Orientation of Coumarin 343 on TiO_2 Surfaces: Application to Dye-Sensitized Solar Cells

Jonathan McCree-Grey,[†,‡] Jacqueline M. Cole,[*,†,§] and Peter J. Evans[‡]

[†]Cavendish Laboratory, Department of Physics, University of Cambridge, J. J. Thomson Avenue, Cambridge CB3 0HE, United Kingdom

[‡]Australian Nuclear Science and Technology Organisation, Lucas Heights, New South Wales 2234, Australia

[§]Argonne National Laboratory, 9700 South Cass Avenue, Argonne, Illinois 60439, United States

Supporting Information

ABSTRACT: The dye···TiO_2 interfacial structure in working electrodes of dye-sensitized solar cells (DSCs) is known to influence its photovoltaic device performance. Despite this, direct and quantitative reports of such structure remain sparse. This case study presents the application of X-ray reflectometry to determine the preferred structural orientation and molecular packing of the organic dye, Coumarin 343, adsorbed onto amorphous TiO_2. Results show that the dye molecules are, on average, tilted by 61.1° relative to the TiO_2 surface, and are separated from each other by 8.2 Å. These findings emulate the molecular packing arrangement of a monolayer of Coumarin 343 within its crystal structure. This suggests that the dye adsorbs onto TiO_2 in one of its lowest energy configurations; that is, dye···TiO_2 self-assembly is driven more by thermodynamic rather than kinetic means. Complementary DSC device tests illustrate that this interfacial structure compromises photovoltaic performance, unless a suitably sized coadsorbant is interdispersed between the Coumarin 343 chromophores on the TiO_2 surface.

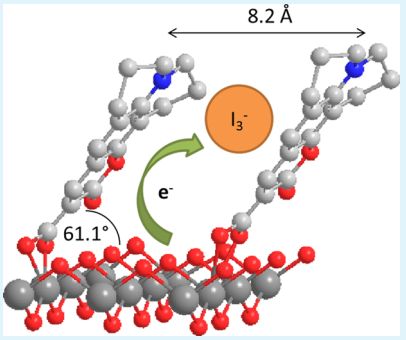

KEYWORDS: *reflectometry, dye-sensitized solar cells, Coumarin 343, molecular orientation*

INTRODUCTION

Since the breakthrough of dye-sensitized solar cells (DSCs) in 1991,[1] the sensitization of titanium dioxide surfaces with photoactive dye molecules has become a topic of intense research interest. A DSC device employs the dye in a dual capacity: as its principal light absorber, rendering the dye in a photoexcited state via sunlight absorption; and as its source of electron current initiation, where the dye injects photoexcited electrons into the conduction band of the semiconducting TiO_2, to which dye molecules are adsorbed. This dye···TiO_2 composite represents the working electrode of the DSC. The structure, orientation, and packing density of dyes at the TiO_2 interface can have a major impact on electron injection processes[2] and bulk TiO_2 surface passivation, thus heavily influencing the overall DSC performance. A variety of materials-characterization techniques that employ spectroscopy,[3−6] diffraction[7] or imaging tools,[8,9] as well as computational methods[10,11] have all been used to infer these dye properties. However, the majority of these effects yield only indirect evidence of interfacial dye···TiO_2 structure. Results from direct physical measurement of dye surfaces remain scarce.

Recently, X-ray reflectometry (XRR) was applied to the successful determination of molecular orientation and packing density for a range of metal-based dye complexes.[12] However, to the best of our knowledge, application of this technique to metal-free organic dyes so far remains unprecedented. Yet, such work is important because organic-dye functionalized DSC devices are now reaching efficiencies comparable to those that embed metal-based dye complexes,[13] and they offer added environmental and synthetic benefits.[14] A better understanding of the interfacial structure of organic dyes, adsorbed onto the surface of TiO_2, is essential for determining how to enhance their associated photovoltaic property attributes. With this in hand, one stands to be able to establish rational molecular design protocols that will yield superior organic dyes for DSC applications.

This Article presents results obtained from XRR studies on the Coumarin 343 dye (C343, $C_{16}H_{15}NO_4$, Figure 1a) when bound to the surface of amorphous TiO_2. The photoelectronic and photophysical properties of C343 have already been investigated extensively: C343 possesses a large molar absorption coefficient, ease of structural modification, high quantum-injection yields, and near-instantaneous electron injection.[15] In principle, these optoelectronic properties make this compound and its chemical derivatives well suited as DSC sensitizers.[16−18] However, it transpires that the overall photovoltaic device efficiency of C343 is low, especially relative to other coumarin-based chromophores.[19] To explore this

Received: April 24, 2015
Accepted: July 10, 2015
Published: July 10, 2015

DOI: 10.1021/acsami.5b03572
ACS Appl. Mater. Interfaces 2015, 7, 16404−16409

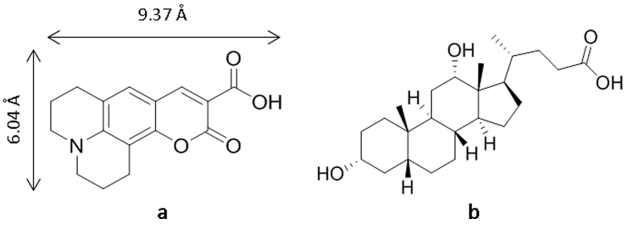

Figure 1. Structures of (a) Coumarin 343 and its corresponding molecular length and width and (b) deoxycholic acid (DCA).

irregularity, the orientation and packing density of C343 about the TiO_2 surface are herein determined and correlated with in-house device performance characteristics of DSCs functionalized by the C343 dye. To this end, the DSC device performance of this dye is enhanced by grafting deoxycholic acid as a coadsorbate. These findings are rationalized within the context of the crystal packing of a monolayer of C343 dye molecules, suggesting that the self-assembly of C343 onto amorphous TiO_2 is dictated by thermodynamic rather than kinetic factors.

METHODS AND MATERIALS

Preparation and Sensitization of Amorphous TiO_2 Thin Films. Amorphous TiO_2 thin films were deposited on silicon (100) wafers, to provide the atomically flat surface required for XRR measurements. This was achieved using an ASM Microchemistry flow-type, hot-walled, F-120 atomic layer deposition (ALD) reactor, which was maintained at 1 mbar pressure and using a deposition temperature of 120 °C. Vaporous $TiCl_4$ and H_2O precursors were delivered from Peltier-cooled reservoirs maintained at 20 °C, following a sequential dosing scheme of 0.4 s $TiCl_4$ exposure, a 1.0 s N_2 purge, a 1.0 s H_2O pulse, and a final 1.5 s N_2 purge.[20] This process was repeated for 200 cycles. A TiO_2 growth rate of ∼0.04 nm/cycle yielded a ∼8 nm thick TiO_2 thin film. The surface appearance of this film was imaged via atomic force microscopy, and its amorphous nature was confirmed by Bragg−Brentano X-ray diffraction measurements.

Prior to dye sensitization, these films were heated to 80 °C for a minimum of 30 min to remove any residual water on their surface. Sensitization was achieved by submersing the TiO_2 films in a 0.3 mM dye solution of C343 (97%, Sigma-Aldrich) in 1:1 acetonitrile:*t*-butanol for 20 h. The resulting films were rinsed with neat acetonitrile and dried under a flow of nitrogen gas prior to being subjected to X-ray reflectometry measurements.

X-ray Reflectometry (XRR). XRR measurements were conducted using a Panalytical X'pert Pro reflectometer that employed a Cu Kα X-ray source (λ = 1.541 Å). The X-ray beam was collimated using a Göbel mirror with a 0.1 mm slit and a postsample parallel collimator. Reflectivity data were collected over a detector range of $0.1° < 2\theta < 10.0°$, incrementing in 0.02° steps, with a count time of 10 s per step. Data were acquired for the TiO_2 substrate before and after its dye sensitization, using the same substrate. The results were refined using the MOTOFIT package[21] for Igor Pro (Wavemetrics) to reveal associated structural parameters, with X-ray reflectivity plotted as a function of the momentum transfer vector (Q) perpendicular to the TiO_2 surface, eq 1.

$$Q = 4\pi\left(\frac{\sin(\theta)}{\lambda}\right) \tag{1}$$

Nominal values for the scattering-length density (SLD) for each layer were used to prepare initial structural models, using a three-layer approach, whereby values of 20.1×10^{-6}, 18.9×10^{-6}, and 31.2×10^{-6} Å^{-2} represented the silicon wafer, the native oxide layer, and TiO_2, respectively. An SLD of 13.6×10^{-6} Å^{-2} was calculated for C343 using eq 2, where r_e refers to the classical electron radius (2.81×10^{-15} m), Z is the sum of atomic numbers (i.e., the total number of electrons) in the C343 molecule (150), and V is the molecular volume of the dye (309.02 Å^3), determined from diffraction data.[22]

$$\mathrm{SLD} = \frac{r_e Z}{V} \tag{2}$$

Dye-Sensitized Solar Cell Device Fabrication and Performance Testing. Working electrodes were fabricated by first depositing two layers of nanoparticulate TiO_2 paste (Dyesol, DSL 18NR-T) onto clean fluorine-doped tin oxide (FTO) glass (TEC7, Dyesol) using the doctor blade method. Sintering of this paste at 500 °C for 30 min yielded ∼10 μm-thick mesoporous TiO_2 films. These films were then submersed in a 0.3 mM 1:1 acetonitrile:*t*-butanol solution of C343 (97% Sigma-Aldrich) for ∼20 h, before being rinsed with neat acetonitrile (Sigma-Aldrich, 99.5% ACS Reagent grade) and dried under a flow of nitrogen. An active dye···TiO_2 working-electrode surface area of ∼1 cm^2 was created via removal of excess TiO_2 from the parent-film periphery.

Counter electrodes were fabricated by first drilling two 0.6 mm diameter holes in clean FTO glass (TEC7, Dyesol). A 5 mM solution of chloroplatinic acid hydrate (Sigma-Aldrich, 99.995%) in isopropanol (Fischer, Analytical reagent grade) was then prepared and drop cast onto the electrodes. These were subsequently heated to 390 °C for 15 min in a box furnace.

Completed cells were assembled by sealing the electrodes together using a thermoplastic gasket (Solaronix, Meltonix 1170-25) and filling the interelectrode volume with an I^-/I_3^- electrolyte solution (Dyesol, EL-HPE) via the predrilled holes. These holes were subsequently blocked using two-part clear epoxy resin (Araldite).

J−*V* curves were measured for each DSC device under illumination using an Abet Technologies Sun 2000 solar simulator (AM1.5G spectrum), calibrated to 1 sun intensity using an Oriel standard silicon reference cell (91150 V). The open-circuit voltage (V_{oc}), short-circuit current density (J_{sc}), and fill-factor (FF) of each cell were determined, from which the power-conversion efficiency (PCE, η) of the device was calculated according to eq 3, where P_{in} refers to the power density of incident-light radiation (100 mW cm^{-2}).

$$\eta = \frac{V_{OC} \cdot J_{SC} \cdot \mathrm{FF}}{P_{in}} \tag{3}$$

Reported DSC device parameters were realized from averaging device performance characteristics from five individual cells (see the Supporting Information) to ensure good reproducibility and accuracy. PCEs are reported both as an absolute quantity as well as a % performance ratio relative to that of DSCs made in-house with N719 dye (ditetrabutylammonium-*cis*-bis(isothiocyanato)bis(2,2′-bipyridyl-4,4′-dicarboxylato)ruthenium(II)). This procedure was adopted because our previous findings show this ratio to be highly consistent across measurements duplicated across a range of laboratory fabrication conditions.[23] This obviates the renowned inconsistencies between absolute PCE values that result from inconsistent J_{sc} data obtained from preparing DSC devices in different laboratories, using different batches of raw materials and varying fabrication personnel.

RESULTS AND DISCUSSION

X-ray Reflectometry (XRR). Figure 2 shows the experimentally observed and fitted XRR data for the C343-sensitized TiO_2 (red trace) and the corresponding untreated TiO_2 substrate (black trace). Structural parameters for the dye-sensitized TiO_2 (SLD; layer thickness; surface roughness) were obtained from model refinements using a three-layer approach, consisting of the dye layer, TiO_2 film, and native oxide layer on the silicon substrate whose SLD and thickness were fixed (Table 1). In contrast, the untreated substrate required only a two-layer model, confirming the absence of any surface contamination such as residual trace amounts of water.[12] Relative to the untreated films, the additional layer in the dye-treated TiO_2 was easily detected due to a large contrast

DOI: 10.1021/acsami.5b03572
ACS Appl. Mater. Interfaces 2015, 7, 16404−16409

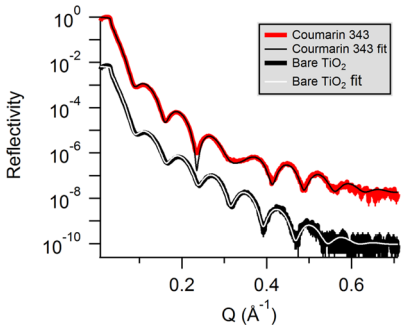

Figure 2. Representative reflectivity profile for Coumarin 343 on an amorphous TiO_2 thin film (red) and the unsensitized TiO_2 thin-film substrate (black). The dye-sensitized substrate results were derived from averaging four sets of raw data (see the Supporting Information).

Table 1. Structural Data for Coumarin 343 on a TiO_2 Thin-Film Substrate, As Determined by Reflectometry Model Refinement[a]

1	2	Coumarin 343
dye layer	formula	$C_{16}H_{15}NO_4$
	thickness/Å	10.0 ± 0.2
	SLD ($\times 10^{-6}$)/Å^{-2}	8.6 ± 0.3
	surface roughness/Å	3.0 ± 0.4
	mass density/g cm^{-3}	0.96
TiO_2 layer	thickness/Å	80.0 ± 0.3
	SLD ($\times 10^{-6}$)/Å^{-2}	30.1 ± 1.0
	interfacial roughness/Å	4.6 ± 0.2

[a]The SLD and thickness of the third layer (SiO_2) were fixed at 5 Å and 18.9 $\times 10^{-6}$ Å^{-2}, respectively, and have been omitted for clarity.

difference between the dye and TiO_2. Under these conditions, the XRR measurements were able to resolve the film thickness with an error of less than 0.2 Å.[12]

An SLD value of 8.6 × 10^{-6} Å^{-2} was observed for C343 on TiO_2. This is 35% lower than the calculated value for pure C343 (13.6 × 10^{-6} Å^{-2}), which suggests a dye layer with low density (0.96 g cm^{-3}; eq 4), relative to that of previously reported dyes, for example, N719 (1.20 g cm^{-3}).[12]

$$\mathrm{SLD} = \frac{r_e N_A \rho Z}{M} \tag{4}$$

where N_A is Avogadro's number, ρ is the mass density, and M is the molecular mass of Coumarin 343 (285.29 u).

The measured average projected area-per-molecule (APM) on the TiO_2 surface is 49.3 Å^2 (eq 5, where d is the dye layer thickness), resulting in a surface concentration, $[\mathrm{dye}]_{\mathrm{surf}}$, of 3.4 × 10^{-10} mol cm^{-2}, eq 6. This is in good agreement with concentrations measured in previous dye adsorption studies on amorphous TiO_2 films.[24]

$$\mathrm{APM} = \frac{r_e Z}{d(\mathrm{SLD})} \tag{5}$$

$$[\mathrm{dye}]_{\mathrm{surf}} = \frac{1}{N_A \times \mathrm{APM}} \tag{6}$$

Similar coumarin derivatives have been shown to bind to the TiO_2 surface via a bidentate chelating carboxylate mode.[16] For modeling purposes, this carboxylate···TiO_2 separation is assumed to be 2.05 Å;[25] this model is consistent with previous spectroscopic results,[26] even though alternative geometries have been speculated via computation.[27] With diffraction data published by Honda et al.,[22] the maximum possible dye-layer thickness corresponds to the sum of this dye···TiO_2 separation and the fully extended length of the dye molecule (Figure 1), that is, the longest dimension of the dye along its molecular mean plane (d_{max} = 11.42 Å). Conceptually, this corresponds to the case where all dye molecules would be aligned perpendicular to the TiO_2 surface. The XRR measurements reveal a dye-layer thickness (d_{obs}) value of 10.0 Å (Table 1), indicating that C343 actually adopts a tilt angle, α, of 61.1 ± 2.3° with respect to the lateral TiO_2 surface, according to basic trigonometric considerations, cf., Figure 3a.

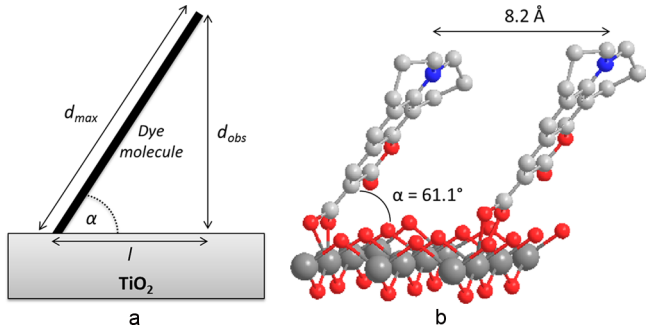

Figure 3. (a) Tilt angle, α, of the dye subtending the TiO_2 surface, calculated from reference to d_{max} and d_{obs} via basic trigonometric considerations; the theoretical area-per-molecule of the dye on the TiO_2 surface calculated by multiplying the molecular width of C343 by $l = d_{max} \cos(\alpha)$. (b) Visualization of C343 molecules bound to the surface. Perpendicular height and intermolecular distance are set in accordance with XRR data.

C343 features a molecular width of 6.04 Å (defined as the distance between atoms O1 and C5 perpendicular to the molecular length (Figure 1), from diffraction data.[22] This indicates a theoretical APM of 33.12 Å^2 (Figure 3a), which is 16.18 Å^2 smaller than the area-per-molecule derived from the measurements using eq 2. Consequently, it is feasible to assume that C343 molecules adopt a special configuration containing an average intermolecular spacing between parallel planes that are separated by 8.2 Å (Figure 3b). This is much larger than anticipated, due to the high propensity of C343 to form $\pi\cdots\pi$ stacking interactions, which should involve an intermolecular distance of approximately 3−4 Å.[28] It should be noted here that this spacing is significantly larger than the longest molecular dimension in I_3^- (~5.27 Å) and acetonitrile (2.59 Å),[29] which means that facile access to the TiO_2 surface should be still be possible. It is therefore reasonable to assume that C343 does not fully passivate the TiO_2 surface, which could lead to a significant reduction in overall cell performance due to unwanted electron decay pathways via electrolyte recombination reactions.[30] It should then offer a reasonable explanation for the low voltage (~0.41 V) obtained by this dye[31] relative to other high-performance dyes such as N3 (*cis*-bis(isothiocyanato) bis(2,2′-bipyridyl-4,4′-dicarboxylato ruthenium(II)),[11] which show higher surface density.[12]

DSC Device Performance. Details on the photovoltaic performance of C343 in a DSC,[31] as well as the effects of incorporating the antiaggregating agent deoxycholic acid (DCA) into DSC devices as a coadsorber to various dyes, have been reported previously.[17,32,33] However, a systematic study of the cooperative effects of pairing C343 and DCA in

DOI: 10.1021/acsami.5b03572
ACS Appl. Mater. Interfaces 2015, 7, 16404−16409

Table 2. Details of the Four Dyeing Methods Employed and Photovoltaic Device Performance Characteristics of C343:DCA Cosensitized DSCs at 1 sun Intensity (AM1.5G Spectrum)[a]

method	dyeing process	V_{OC}/V	J_{SC}/mA cm^{-2}	FF/%	PCE/%	N719 performance ratio/%
A	0.3 mM C343 for 20 h	0.27 ± 0.03	0.09 ± 0.01	41.1 ± 0.9	0.010 ± 0.002	0.3
B	as for "A", but repeated for further 20 h	0.28 ± 0.03	0.10 ± 0.01	40.2 ± 0.7	0.011 ± 0.001	0.3
C	mixture of 0.3 mM C343 and 0.2 mM DCA for 20 h	0.333 ± 0.004	0.12 ± 0.01	44.3 ± 0.4	0.018 ± 0.001	0.5
D	0.3 mM C343 for 20 h, then subsequently 0.2 mM DCA for 20 h	0.39 ± 0.03	0.15 ± 0.02	48.0 ± 1.5	0.027 ± 0.008	0.7

[a]The N719 performance ratio is calculated using an internal-reference N719 device efficiency obtained by the authors (3.7%) to normalize the subject results; see the Supporting Information.

DSC devices is unprecedented, to the best of our knowledge. Systematic investigation of the effects of such cosensitization on photovoltaic behavior stands to provide some further insight into the nature of the dye···TiO_2 interfacial structure observed via XRR; in particular, a rationale behind the larger-than-expected C343 intermolecular distance. C343-based DSC devices were fabricated with the photoinactive DCA coadsorbate according to one of four dyeing methods, as outlined in Table 2; 1:1 acetonitrile:*t*-butanol was used as the solvent throughout. DCA (Figure 1b) was chosen on the basis of its similarity in size and shape to C343, and the lack of discernible planar π-moieties, ensuring passivation to electronic intermolecular interactions.

DSCs obtained from method A exhibited a power conversion efficiency (PCE, η) of 0.010% (Table 2; Figure 4), which is low

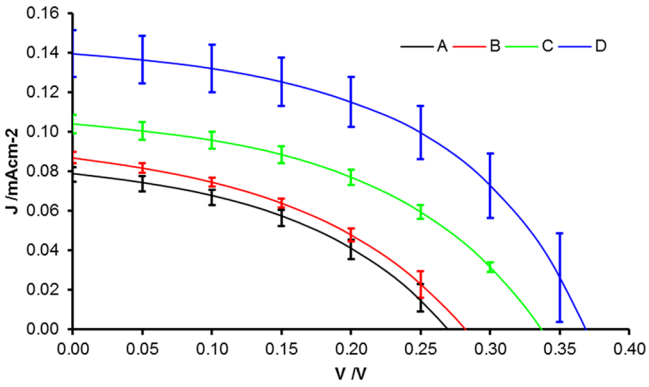

Figure 4. *J*–*V* curves for DSCs resulting from method A (black), method B (red), method C (green), and method D (blue).

compared to literature values, and should be attributed to the simplified fabrication process used for this work.[31] Exposing devices to a more lengthy dyeing process (e.g., method B) did not affect their performance significantly, indicating saturated surface coverage, with respect to C343 after the first cycle.

Devices obtained from method C showed a significantly higher PCE, resulting predominantly from an improvement in V_{OC} and J_{SC} (see Table 2; Figure 4). The highest performance was achieved when using method D, with an almost 3-fold increase in PCE over devices following methods A or B. The V_{oc} = 0.386 V attained was attributed to a reduction in recombination reactions due to improved surface passivation.[34] J_{SC} also increased to 0.15 mA cm^{-2}, and FF went up to 48.0%. This is attributable to a positive shift of the TiO_2 conduction-band edge in the presence of DCA, and suppression of quenching processes, resulting in increased electron-injection yields.[34] Both of these effects indicate successful coadsorption of DCA to the TiO_2 surface (Figure 5). This DSC fabrication

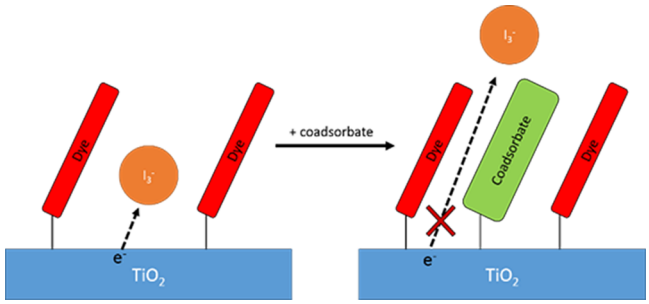

Figure 5. Schematic diagram showing the approach of the I_3^- to the TiO_2 surface and inducing recombination with electrons in the TiO_2 conduction band (left); and (right) how the inclusion of a coadsorbate can prevent this recombination.

method also ensured that DCA coadsorption was not accompanied by concurrent C343 desorption, as evidenced by the colorless DCA solutions that persisted upon the coadsorbant sensitization step in the sequential dyeing process; contamination from C343 would afford a green solution. As DCA adsorption occurs after C343 sensitization, and no C343 desorption was observed, these results support the XRR results, which indicate that sufficient space should exist between the dye molecules to allow DCA to adsorb. As repeated sensitization with C343 yielded insignificant improvement in the device efficiency as compared to devices containing DCA, it is reasonable to assume that the limiting factor for the dye adsorption is the electronic interaction between the π-electrons in the C343 molecules, rather than steric congestion with respect to the surface, which may be expected intuitively.

A Proposed Justification for the Dye···TiO_2 Interfacial Structure Observed by XRR. Considering these XRR and DSC device results, along with a priori knowledge of the behavior of C343 in the solid state and in solution, a possible justification for the larger-than-expected intermolecular spacing of C343 molecules can be proposed. Previous studies have focused on the behavior of C343 in solution and have shown J-aggregates in the presence of nonpolar solvents.[35] However, details surrounding the possible formation of H-aggregates of this dye, and of DSC dyes generally, are less well-known. One example by Nuesch and Grätzel has shown that the H-aggregation of merocyanine dyes, formed upon adsorption onto TiO_2 nanoparticle surfaces, presents a configuration similar to the crystal packing of the dye.[36] When one considers the crystal structure of C343 (Figure 6),[22] a distinct layering is observable along the *c*-axis of the unit cell, with carboxylic-acid groups on adjacent molecules facing alternating directions.

The intermolecular distance between these molecular layers is 3.5(4) Å, consistent with parallel displaced π···π stacking.[28] By taking just a single layer of molecules (Figure 6, shaded

DOI: 10.1021/acsami.5b03572
ACS Appl. Mater. Interfaces 2015, 7, 16404–16409

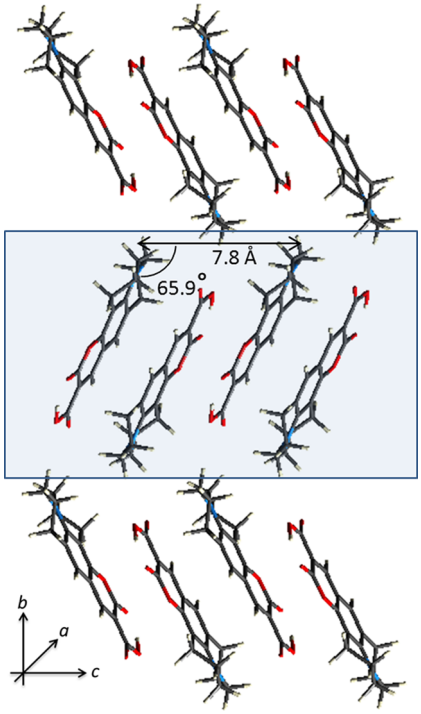

Figure 6. Crystal structure of C343[22] looking down the *a*-axis of the unit cell. Image generated using CrystalExplorer, Version 3.1.[37]

box), it is also observable that the intermolecular distance between molecules of the same orientation is 7.8(4) Å and has an angle relative to each other of 65.9(6)°. These observations are very close to the values of 8.2 Å and 61.1° for C343 on TiO_2 as derived from XRR results. It would therefore seem that, close to the TiO_2 surface, a similar molecular arrangement is occurring, with every other molecule being of an unfavorable orientation to formulate a bond between its carboxylic acid and TiO_2. This may also be influenced by adsorption of solvent molecules to the surface. In either case, the eventual removal of these nonadsorbed species, during the cell fabrication process, would result in molecular orientation and packing as measured by XRR. While the surface structure inferences of dye packing on TiO_2 from XRR were also compared to other molecular layer configurations in the C343 crystal structure (see the Supporting Information), their good correspondence with molecular layers along the *c*-axis was unique.

This link between crystal structure and dye···TiO_2 surface structure has significant implications for the energetics associated with self-assembly of dye molecules adsorbing onto TiO_2. The crystal structure of a material is naturally one of, if not, the lowest-energy configurations of a molecule. The rationale for this is the need for a driving energy that overcomes a decrease in free energy to induce crystallization. Accordingly, crystal structures are most commonly represented by the most thermodynamically stable state of the molecule. The fact that the XRR-derived parametrics of the dye···TiO_2 interfacial structure relate so closely to that of a monolayer of the C343 crystal structure along the *c*-axis indicates a thermodynamic mechanism behind dye···TiO_2 self-assembly. At first sight, this might seem counterintuitive given that dye molecules are drawn to the TiO_2 surface somewhat dynamically given that they reside in a solution environment. Yet, dye···TiO_2 interfaces and the associated dye loading onto TiO_2 are poorly understood. So it is entirely possible that local-field forces associated with the dye are substantially modulated as they approach the TiO_2 surface, to the extent that they emulate crystal-field forces. As such, dye···TiO_2 self-assembly could readily be controlled by thermodynamic rather than kinetic origins, as indicated by the XRR results herein. This proposed self-assembly mechanism not only rationalizes the poor DSC performance of C343 relative to other coumarin derivatives, but is also entirely consistent with the observed improvement in DSC photovoltaic output once a DCA coadsorbant was added to fill the interstices, which would form as a result of thermodynamically driven self-assembly.

CONCLUSIONS

The interfacial structure of the Coumarin 343 dye···TiO_2 composite, that forms the working electrode of a DSC, has been determined by X-ray reflectometry. The molecular orientation and packing of the dye on the TiO_2 surface have been quantified, revealing that C343 dyes self-assemble on TiO_2 via thermodynamic rather than kinetic energy constraints. The large lateral dye···dye separation (8.2 Å) on C343-sensitized TiO_2 working electrode surfaces that is observed has significant implications for the photovoltaic device performance of the corresponding DSCs. In its native state, inefficient dye loading onto the TiO_2 surface is afforded, exposing the working electrode to electrolyte-to-TiO_2-based electron recombination, and compromising electron injection; this explains the poor device efficiency of C343-based DSCs. Fortunately, this situation can be rectified by cosensitizing the C343-based DSC with deoxycholic acid, which fills the interstices on the TiO_2 surface that arose from the thermodynamically driven C343 self-assembly process.

ASSOCIATED CONTENT

Supporting Information

Tables of photovoltaic device performance characteristics from individual tests of multiplicate DSCs prior to their averaging; raw XRR data for the dye-sensitized substrate; modeled structural parameters for the bare TiO_2 film; and further discussion of surface structure versus crystal structure configurations. The Supporting Information is available free of charge on the ACS Publications website at DOI: 10.1021/acsami.5b03572.

AUTHOR INFORMATION

Corresponding Author

*E-mail: jmc61@cam.ac.uk.

Notes

The authors declare no competing financial interest.

ACKNOWLEDGMENTS

We wish to thank Stephen Holt from ANSTO for induction on X-ray reflectometry instrumentation at OPAL, and also Andrew Nelson and Gerry Triani for their guidance on data analysis and TiO_2 deposition, respectively. J.M-G. acknowledges ANSTO for a part-funded Ph.D. studentship. J.M.C. is grateful to the 1851 Royal Commission for the 2014 Design Fellowship, and Argonne National Laboratory where work done was supported by DOE Office of Science, Office of Basic Energy Sciences, under contract no. DE-AC02-06CH11357.

DOI: 10.1021/acsami.5b03572
ACS Appl. Mater. Interfaces 2015, 7, 16404−16409

REFERENCES

(1) O'Regan, B.; Gratzel, M. A Low-Cost High-Efficiency Solar Cell Based on Dye-Sensitized Colloidal TiO_2 Films. *Nature* **1991**, *353*, 737−740.

(2) Katoh, R.; Furube, A. Electron Injection Efficiency in Dye-Sensitized Solar Cells. *J. Photochem. Photobiol., C* **2014**, *20* (0), 1−16.

(3) Marinado, T.; Hagberg, D. P.; Hedlund, M.; Edvinsson, T.; Johansson, E. M. J.; Boschloo, G.; Rensmo, H.; Brinck, T.; Sun, L.; Hagfeldt, A. Rhodanine Dyes for Dye-Sensitized Solar Cells: Spectroscopy, Energy Levels and Photovoltaic Performance. *Phys. Chem. Chem. Phys.* **2009**, *11* (1), 133−141.

(4) Brennan, T. P.; Tanskanen, J. T.; Bakke, J. R.; Nguyen, W. H.; Nordlund, D.; Toney, M. F.; McGehee, M. D.; Sellinger, A.; Bent, S. F. Dynamical Orientation of Large Molecules on Oxide Surfaces and its Implications for Dye-Sensitized Solar Cells. *Chem. Mater.* **2013**, *25* (21), 4354−4363.

(5) Deacon, G. B.; Phillips, R. J. Relationships Between the Carbon-Oxygen Stretching Frequencies of Carboxylato Complexes and the Type of Carboxylate Coordination. *Coord. Chem. Rev.* **1980**, *33* (3), 227−250.

(6) Pérez León, C.; Kador, L.; Peng, B.; Thelakkat, M. Characterization of the Adsorption of Ru-bpy Dyes on Mesoporous TiO_2 Films with UV−Vis, Raman, and FTIR Spectroscopies. *J. Phys. Chem. B* **2006**, *110* (17), 8723−8730.

(7) Zubavichus, Y. V.; Slovokhotov, Y. L.; Nazeeruddin, M. K.; Zakeeruddin, S. M.; Grätzel, M.; Shklover, V. Structural Characterization of Solar Cell Prototypes Based on Nanocrystalline TiO_2 Anatase Sensitized with Ru Complexes. X-ray Diffraction, XPS, and XAFS Spectroscopy Study. *Chem. Mater.* **2002**, *14* (8), 3556−3563.

(8) Kley, C. S.; Dette, C.; Rinke, G.; Patrick, C. E.; Čechal, J.; Jung, S. J.; Baur, M.; Dürr, M.; Rauschenbach, S.; Giustino, F.; Stepanow, S.; Kern, K. Atomic-Scale Observation of Multiconformational Binding and Energy Level Alignment of Ruthenium-Based Photosensitizers on TiO_2 Anatase. *Nano Lett.* **2014**, *14* (2), 563−569.

(9) Sasahara, A.; Pang, C. L.; Onishi, H. STM Observation of a Ruthenium Dye Adsorbed on a TiO_2(110) Surface. *J. Phys. Chem. B* **2006**, *110* (10), 4751−4755.

(10) Pastore, M.; De Angelis, F. Intermolecular Interactions in Dye-Sensitized Solar Cells: A Computational Modeling Perspective. *J. Phys. Chem. Lett.* **2013**, *4* (6), 956−974.

(11) Nazeeruddin, M. K.; De Angelis, F.; Fantacci, S.; Selloni, A.; Viscardi, G.; Liska, P.; Ito, S.; Takeru, B.; Grätzel, M. Combined Experimental and DFT-TDDFT Computational Study of Photoelectrochemical Cell Ruthenium Sensitizers. *J. Am. Chem. Soc.* **2005**, *127* (48), 16835−16847.

(12) Griffith, M. J.; James, M.; Triani, G.; Wagner, P.; Wallace, G. G.; Officer, D. L. Determining the Orientation and Molecular Packing of Organic Dyes on a TiO_2 Surface Using XRR. *Langmuir* **2011**, *27*, 12944−12950.

(13) Xiang, W.; Huang, W.; Bach, U.; Spiccia, L. Stable High Efficiency Dye-Sensitized Solar Cells Based on a Cobalt Polymer Gel Electrolyte. *Chem. Commun.* **2013**, *49* (79), 8997−8999.

(14) Mishra, A.; Fischer, M. K. R.; Bäuerle, P. Metal-Free Organic Dyes for Dye-Sensitized Solar Cells: From Structure: Property Relationships to Design Rules. *Angew. Chem., Int. Ed.* **2009**, *48* (14), 2474−2499.

(15) Liu, X.; Cole, J. M.; Waddell, P. G.; Lin, T.-C.; McKechnie, S. Molecular Origins of Optoelectronic Properties in Coumarins 343, 314T, 445, and 522B. *J. Phys. Chem. C* **2013**, *117* (27), 14130−14141.

(16) Wang, Z.-S.; Hara, K.; Dan-oh, Y.; Kasada, C.; Shinpo, A.; Suga, S.; Arakawa, H.; Sugihara, H. Photophysical and (Photo)-electrochemical Properties of a Coumarin Dye. *J. Phys. Chem. B* **2005**, *109* (9), 3907−3914.

(17) Wang, Z.-S.; Cui, Y.; Dan-oh, Y.; Kasada, C.; Shinpo, A.; Hara, K. Thiophene-Functionalized Coumarin Dye for Efficient Dye-Sensitized Solar Cells: Electron Lifetime Improved by Coadsorption of Deoxycholic Acid. *J. Phys. Chem. C* **2007**, *111* (19), 7224−7230.

(18) Liu, X.; Cole, J. M.; Waddell, P. G.; Lin, T.-C.; Radia, J.; Zeidler, A. Molecular Origins of Optoelectronic Properties in Coumarin Dyes: Toward Designer Solar Cell and Laser Applications. *J. Phys. Chem. A* **2012**, *116* (1), 727−737.

(19) Hara, K.; Kurashige, M.; Dan-oh, Y.; Kasada, C.; Shinpo, A.; Suga, S.; Sayama, K.; Arakawa, H. Design of New Coumarin Dyes Having Thiophene Moieties for Highly Efficient Organic-Dye-Sensitized Solar Cells. *New J. Chem.* **2003**, *27* (5), 783−785.

(20) Triani, G.; Campbell, J. A.; Evans, P. J.; Davis, J.; Latella, B. A.; Burford, R. P. Low Temperature Atomic Layer Deposition of Titania Thin Films. *Thin Solid Films* **2010**, *518* (12), 3182−3189.

(21) Nelson, A. Co-refinement of Multiple-Contrast Neutron/X-ray Reflectivity Data Using MOTOFIT. *J. Appl. Crystallogr.* **2006**, *39* (2), 273−276.

(22) Honda, T.; Fujii, I.; Hirayama, N.; Aoyama, N.; Miike, A. Coumarin 343, $C_{16}H_{15}NO_4$. *Acta Crystallogr., Sect. C: Cryst. Struct. Commun.* **1996**, *C52*, 679−681.

(23) Cole, J. M.; Low, K. S.; Ozoe, H.; Stathi, P.; Kitamura, C.; Kurata, H.; Rudolf, P.; Kawase, T. Data Mining with Molecular Design Rules Identifies New Class of Dyes for Dye-Sensitised Solar Cells. *Phys. Chem. Chem. Phys.* **2014**, *16* (48), 26684−26690.

(24) Harms, H. A.; Tetreault, N.; Gusak, V.; Kasemo, B.; Gratzel, M. In Situ Investigation of Dye Adsorption on TiO_2 Films Using a Quartz Crystal Microbalance With a Dissipation Technique. *Phys. Chem. Chem. Phys.* **2012**, *14* (25), 9037−9040.

(25) Schiffmann, F.; VandeVondele, J.; Hutter, J. R.; Wirz, R.; Urakawa, A.; Baiker, A. Protonation-Dependent Binding of Ruthenium Bipyridyl Complexes to the Anatase(101) Surface. *J. Phys. Chem. C* **2010**, *114* (18), 8398−8404.

(26) Jiang, L.-l.; Liu, W.-L.; Song, Y.-F.; He, X.; Wang, Y.; Wu, H.-L.; Yang, Y.-Q. Fluorescence and Raman Spectroscopic Characteristics of the Photo-Induced Electron Transfer of Coumarin 343 Dye-Sensitized TiO_2 Nanoparticles. *Acta Phys. Chim. Sin.* **2012**, *28* (12), 2953−2957.

(27) Yang, L.; Wu, W.; Zhao, Y. Effect of TiO_2 Particles on Normal and Resonance Raman Spectra of Coumarin 343: A Theoretical Investigation. *Phys. Chem. Chem. Phys.* **2015**, *17* (16), 10910−10918.

(28) Janiak, C. A Critical Account on π-π Stacking in Metal Complexes with Aromatic Nitrogen-Containing Ligands. *J. Chem. Soc., Dalton Trans.* **2000**, *21*, 3885−3896.

(29) Olejniczak, A.; Katrusiak, A. Supramolecular Reaction between Pressure-Frozen Acetonitrile Phases α and β. *J. Phys. Chem. B* **2008**, *112* (24), 7183−7190.

(30) Pascoe, A. R.; Bourgeois, L.; Duffy, N. W.; Xiang, W.; Cheng, Y.-B. Surface State Recombination and Passivation in Nanocrystalline TiO_2 Dye-Sensitized Solar Cells. *J. Phys. Chem. C* **2013**, *117* (47), 25118−25126.

(31) Hara, K.; Sato, T.; Katoh, R.; Furube, A.; Ohga, Y.; Shinpo, A.; Suga, S.; Sayama, K.; Sugihara, H.; Arakawa, H. Molecular Design of Coumarin Dyes for Efficient Dye-Sensitized Solar Cells. *J. Phys. Chem. B* **2003**, *107* (2), 597−606.

(32) Feng, Q.; Wang, H.; Zhou, G.; Wang, Z.-S. Effect of Deoxycholic Acid on Performance of Dye-Sensitized Solar Cell Based on Black Dye. *Front. Optoelectron.* **2011**, *4* (1), 80−86.

(33) Sharma, G. D.; Kurchania, R.; Ball, R. J.; Roy, M. S.; Mikroyannidis, J. A. Effect of Deoxycholic Acid on the Performance of Liquid Electrolyte Dye-Sensitized Solar Cells Using a Perylene Monoimide Derivative. *Int. J. Photoenergy* **2012**, *2012*, 7.

(34) Hara, K.; Dan-oh, Y.; Kasada, C.; Ohga, Y.; Shinpo, A.; Suga, S.; Sayama, K.; Arakawa, H. Effect of Additives on the Photovoltaic Performance of Coumarin-Dye-Sensitized Nanocrystalline TiO_2 Solar Cells. *Langmuir* **2004**, *20* (10), 4205−4210.

(35) Liu, X.; Cole, J. M.; Low, K. S. Molecular Origins of Dye Aggregation and Complex Formation Effects in Coumarin 343. *J. Phys. Chem. C* **2013**, *117* (28), 14723−14730.

(36) Nüesch, F.; Grätzel, M. H-aggregation and Correlated Absorption and Emission of a Merocyanine Dye in Solution, at the Surface and in the Solid State. A Link Between Crystal Structure and Photophysical Properties. *Chem. Phys.* **1995**, *193* (1−2), 1−17.

(37) Wolff, S. K.; Grimwood, D. J.; McKinnon, J. J.; Turner, M. J.; Jayatilaka, D.; Spackman, M. A. *Crystal Explorer 3.1*; University of Western: Australia, 2012.

DOI: 10.1021/acsami.5b03572
ACS Appl. Mater. Interfaces 2015, 7, 16404−16409